AIAA JOURNAL
Vol. 42, No. 6, June 2004

Mechanics and Finite Element for Nonlinear Response of Active Laminated Piezoelectric Plates

Dimitris Varelis* and Dimitris A. Saravanos†
University of Patras, GR26500 Patras, Greece

A theoretical framework for analyzing piezoelectric composite laminates that includes nonlinear effects as a result of large displacements and rotations is presented. Nonlinear mechanics equations are incorporated into a coupled mixed-field piezoelectric laminate theory. Using the nonlinear laminate theory, a nonlinear finite element methodology and an incremental-iterative solution are formulated for the analysis of nonlinear adaptive laminated plate structures with piezoelectric actuators and sensors. An eight-node nonlinear plate finite element is also developed. The mechanics models are applied on the nonlinear active response of composite plates with piezoelectric actuators. Various application cases quantify the nonlinear active flexural response of beams and plates with piezoelectric actuators.

Nomenclature

A, B, D	=	generalized laminate stiffness matrices
b	=	body force
C	=	elastic stiffness
D	=	electric displacement
d	=	incremental operator
E	=	electric field
$\bar{E}^m, \hat{E}^m$	=	generalized laminate piezoelectric matrices
e	=	piezoelectric coefficients
F	=	external mechanical force
G^{mn}	=	generalized laminate permittivity matrices
K^L	=	nonlinear matrix
K^o	=	linear matrix
K^σ	=	initial stress matrix
$\bar{K}$	=	tangential stiffness matrices
k	=	curvature
N	=	in-plane interpolation functions
P_1, P_2	=	nonlinear stiffness matrix depending on linear and quadratic displacements
P_3, P_4	=	converse and direct nonlinear piezoelectric matrix depending on linear displacements
Q	=	external electric charge
S	=	strain
u, v, w	=	displacements along x, y, z axes
x, y, z	=	coordinate axes
β_x, β_y	=	rotation angles
δ	=	variational operator
ε	=	electric permittivity
σ	=	stress
$\bar{\tau}, \bar{q}$	=	prescribed surface traction and charge
φ	=	electric potential
Ψ^m	=	through-thickness interpolation functions
Ψ_e	=	nodal charge imbalance
Ψ_u	=	nodal force imbalance

Subscripts

L	=	nonlinear terms
uu, ue, eu, ee	=	structural, converse piezoelectric, direct piezoelectric, dielectric
x, y, z	=	x, y, z component
1, 2, 3	=	normal components
4, 5, 6	=	out-of-plane and in-plane shear component
,	=	differentiation

Superscripts

E	=	constant electric field conditions
m, n	=	layerwise component
o	=	terms referred on midsurface
S	=	constant strain conditions

Introduction

DURING the recent years, the study of piezoelectric composite materials of smart/adaptive piezoelectric structures has received substantial attention. Numerous analytical and computational models for smart/adaptive piezoelectric structures using various theories have been reported,[1] but the majority of them have been limited to the linear region and have been mainly focused on the static and dynamic response of smart structures. For example, early work has been reported on linear induced-strain Kirchhoff and first-order shear models for plates[2,3] and shells.[4] Uncoupled layerwise beam models[5] and uncoupled higher-order plate finite elements[6] were presented. Coupled linear plate and shells models were also developed using full layerwise[7] or mixed single-layer layerwise mechanics models and finite elements.[8,9] Exact linear static and dynamic solutions for various plate geometries have been also reported.[10,11] However, among the many issues that have surfaced so far, one is that in many applications the severity and type of electromechanical loading can exceed the linear range, thus inducing nonlinear behavior and new modes of failure such as buckling or structural stability problems. Another issue is the initiative for developing adaptive structures capable of undergoing large deformations, such as morphing structures. This paper addresses some of these needs in current technology, by presenting a nonlinear mechanics formulation and a finite element solution for the analysis of piezoelectric-composite laminated beams and plates undergoing large rotations and deflections.

Limited in scope, work has been reported thus far on the nonlinear response of piezoelectric structures. In the area of nonlinear material behavior, Fripp and Hagood[12] reported a theoretical framework for the dynamic response of electrostrictive actuators, and Debus et al.[13] presented a finite element model for the static analysis of electrostrictive actuators. Lee and Saravanos[14] developed layerwise mechanics equations and a finite element method for thermal

Presented as Paper 2002-1442 at the AIAA/ASME/ASCE/AHS/ASC 43rd Structures, Structural Dynamics, and Materials Conference and 10th Adaptive Structures Conference, Denver, CO, 22–25 April 2002; received 30 December 2002; revision received 23 October 2003; accepted for publication 6 January 2004.

*Graduate Research Assistant, Department of Mechanical Engineering and Aeronautics.

†Associate Professor, Department of Mechanical Engineering and Aeronautics; saravanos@mech.upatras.gr. Associate Fellow AIAA.

piezocomposite plates with temperature-varying material properties. Thornburgh and Chattopadhyay[15] reported high-order models for the behavior of active plates using nonlinear piezoelectric terms. In the area of geometric nonlinearity of piezoelectric structures, Pai et al.[16] reported an uncoupled induced-strain nonlinear theory for the dynamics and active control of piezoelectric plates, Tzou and coworkers[17,18] reported uncoupled theoretical formulations for thermopiezoelectric plates and for the active control of nonlinear deflections, Oh et al.[19] presented an uncoupled layerwise finite element for postbuckling of thermopiezoelectric plates, and Mukherjee and Chaudhouri[20] investigated the nonlinear response of a cantilever bimorph beam.

The present paper presents a generalized efficient multifield nonlinear mechanics theory and a finite element type for the analysis of piezocomposite laminates and plates, which include nonlinear effects caused by large displacements and rotations. The development of a coupled nonlinear piezoelectric laminate theory that uses both displacements and electric potential as field variables is first described. Governing nonlinear equations are presented and are subsequently combined with mixed-field shear-layerwise kinematic assumptions.[8] Discrete nonlinear equations of motion are formulated for piezoelectric plate structures in combination with an in-plane finite element approximation. An incremental-iterative technique, based on Newton–Raphson solution method,[21] is formulated next. Discrete linearized equations of motion are derived, and the new tangential and nonlinear system matrices and terms are enumerated. Finally, a parabolic nonlinear piezocomposite plate element is developed. The nonlinear static response of active piezocomposite plates, subject to combined flexural mechanical and electric loads, is subsequently investigated. Various numerical results from evaluations and applications of the method on active beams and plates subject to large quasi-static out-of-plane electromechanical loads are shown. The contribution of new terms on the nonlinear response is also illustrated.

Laminate Mechanics

Governing Equations

The material of each ply of the piezoelectric laminate is assumed to remain within the range of linear piezoelectricity, with constitutive equations of the form

$$\sigma_i = C_{ij}^E S_j - e_{ik} E_k, \qquad D_l = e_{lj} S_j + \varepsilon_{lk}^S E_k \tag{1}$$

where $i,\ j = 1, \ldots, 6$ and $k, l = 1, \ldots, 3$; σ_i and S_j are the mechanical stresses and engineering strains in extended vectorial notation, C_{ij} is the elastic stiffness tensor, e_{ik} is the piezoelectric tensor, E_k is the electric field vector, D_l is the electric displacement vector, and ε_{lk} is the electric permittivity tensor. The preceding equations describe the material behavior either on the orthogonal material axes 1, 2, 3 or the structural axes x, y, and z, respectively, provided that proper transformations are applied on material property matrices.

The Green–Lagrange strains in each ply are assumed to have the following form:

$$S_1 = u_{,x} + \tfrac{1}{2} w_{,x}^2, \qquad S_2 = v_{,y} + \tfrac{1}{2} w_{,y}^2$$
$$S_6 = (u_{,y} + v_{,x}) + w_{,x} w_{,y}, \qquad S_4 = u_{,z} + w_{,x}$$
$$S_5 = v_{,z} + w_{,y}, \qquad S_3 = 0 \tag{2}$$

where the first right-hand-side (RHS) terms describe the linear strain components and the last RHS terms are the nonlinear strain components caused by large out-of-plane rotations, respectively.

Kinematic Assumptions

The coupled mixed-field laminate theory[8] kinematic assumptions are used, which combine a linear displacement field with a discrete-layer electric potential field, thus representing all state variables through the laminate thickness. The discrete-layer field divides the laminate into L-1 sublaminates and assumes a continuous electric potential field through each sublaminate, such that a piecewise continuous field results through the whole thickness of the piezolaminate, as seen in Fig. 1. The assumed displacements and electric potential have the following form through the thickness:

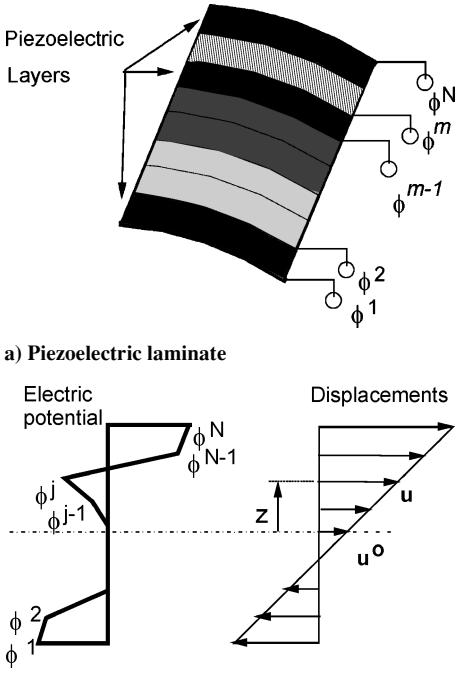

Fig. 1 Piezoelectric laminates: a) mixed-field kinematic assumptions and b) assumed through-the-thickness displacement and electric potentials fields.

$$u(x, y, z, t) = u^o(x, y, t) + z\beta_x(x, y, t)$$
$$v(x, y, z, t) = v^o(x, y, t) + z\beta_y(x, y, t)$$
$$w(x, y, z, t) = w^o(x, y, t)$$
$$\varphi(x, y, z, t) = \sum_{m=1}^{L} \varphi^m(x, y, t)\Psi^m(z) \tag{3}$$

where u^o, v^o, w^o are midsurface displacements, β_x and β_y are rotation angles, ϕ^m are electric potential values describing the layerwise electric potential field, and Ψ^m are linear interpolation functions. In the context of the preceding kinematic assumptions [Eq. (3)] and nonlinear strain relations [Eq. (2)], the strains through the thickness of the laminate take the following form:

$$\begin{Bmatrix} S_1 \\ S_2 \\ S_6 \end{Bmatrix} = \begin{Bmatrix} S_1^0 \\ S_2^0 \\ S_6^0 \end{Bmatrix} + z \begin{Bmatrix} k_1^0 \\ k_2^0 \\ k_6^0 \end{Bmatrix} + \begin{Bmatrix} S_{L1} \\ S_{L2} \\ S_{L6} \end{Bmatrix}, \qquad \begin{Bmatrix} S_{s4} \\ S_{s5} \end{Bmatrix} = \begin{Bmatrix} S_{s4}^0 \\ S_{s5}^0 \end{Bmatrix} \tag{4}$$

where $i = 1, 2, 6$ and $j = 4, 5$; S_i^0, S_{sj}^0 are midinplane and shear strains, respectively, and k_i^0 midsurface curvatures[8]; S_{Li} are the nonlinear laminate strains on the midsurface, which are expressed here:

$$S_{L1} = \tfrac{1}{2} w_{,x}^{o2} \qquad S_{L2} = \tfrac{1}{2} w_{,y}^{o2} \qquad S_{L6} = w_{,x}^o \cdot w_{,y}^o \tag{5}$$

The electric field vector has the form

$$E_i(x, y, \zeta, t) = \sum_{m=1}^{L} E_i^m(x, y, t)\Psi^m(\zeta), \qquad i = 1, 2$$
$$E_3(x, y, \zeta, t) = \sum_{m=1}^{L} E_3^m(x, y, t)\Psi_{,\zeta}^m(\zeta) \tag{6}$$

where the generalized electric field vector E^m is defined as

$$E_1^m = -\Phi_{,x}^m, \qquad E_2^m = -\Phi_{,y}^m, \qquad E_3^m = -\Phi^m \tag{7}$$

Generalized Equations of Motion

The mechanical and electrical equilibrium of the laminated plate are represented by the stress equilibrium and the conservation of electric charge equations, respectively. Through the use of the divergence theorem, the latter can be expressed by the equivalent variational forms shown in the RHS of the following equations:

$$\{\delta u\}^T\{\Psi_u\} = -\int_V \delta S_i \sigma_i \,\mathrm{d}V + \int_V \delta u_j b_j \,\mathrm{d}V + \int_{\Gamma_\tau} \delta\bar{u}_j \bar{\tau}_j \,\mathrm{d}\Gamma = 0$$

$$\{\delta\varphi\}^T\{\Psi_e\} = -\int_V \delta E_j D_j \,\mathrm{d}V + \int_{\Gamma_q} \delta\bar{\varphi}\bar{q} \,\mathrm{d}\Gamma = 0$$

$$i = 1, \ldots, 6, \qquad j = 1, \ldots, 3 \tag{8}$$

The vectors Ψ_u, Ψ_e represent differences between internal and external forces and charges, respectively, which diminish at equilibrium; $\bar{\tau}$ are the surface tractions on the bounding surface Γ_τ, $\bar{q}$ is the electrical charge applied on the terminal bounding surface Γ_q; and V represents the whole laminate volume including both composite and piezoelectric layers. Combining Eq. (8) with Eqs. (4–6), integrating through the thickness of the piezocomposite laminate, and collecting the common generalized strain and electric field terms, equivalent variational forms are finally derived at the laminate level:

$$\begin{aligned}\{\delta u\}^T\{\Psi_u\} = -\int_{A_o} \Big(& \{\delta S^o\}^T[A]\{S^o\} + \{\delta S^o\}^T[B]\{k^o\} \\ & + \{\delta k^o\}^T[B]\{S^o\} + \{\delta k^o\}^T[D]\{k^o\} + \left\{\delta S_s^o\right\}^T[A_s]\left\{S_s^o\right\} \\ & + \{\delta S^L\}^T[A]\{S^o\} + \{\delta S^L\}^T[A]\{S^L\} + \{\delta S^L\}^T[B]\{k^o\} \\ & + \{\delta S^o\}^T[A]\{S^L\} + \{\delta k^o\}^T[B]\{S^L\} + \sum_m \{\delta S^o\}^T[\bar{E}^m]\{E^m\} \\ & + \sum_m \{\delta k^o\}^T[\hat{E}^m]\{E^m\} + \sum_m \{\delta S^L\}^T[\bar{E}^m]\{E^m\} \Big) \,\mathrm{d}A \\ & + \int_{\Gamma_\tau} \{\delta u\}^T\{\bar{\tau}\} \,\mathrm{d}\Gamma = 0\end{aligned}$$

$$\begin{aligned}\{\delta\varphi\}^T\{\Psi_e\} = -\int_{A_o} \Big(& \sum_m \{\delta E^m\}^T[\bar{E}^m]\{S^o\} + \sum_m \{\delta E^m\}^T[\hat{E}^m]\{k^o\} \\ & + \sum_m \{\delta E^m\}^T[\bar{E}^m]\{S^L\} + \sum_{mn} \{\delta E^m\}^T[G^{mn}]\{E^n\} \Big) \,\mathrm{d}A \\ & + \int_{\Gamma_q} \{\delta\varphi\}^T\{\bar{q}\} \,\mathrm{d}\Gamma = 0, \qquad m, n = 1, \ldots, L\end{aligned} \tag{9}$$

The first equation mandates the mechanical equilibrium of an active laminate, where the first line contains linear terms, the second nonlinear terms, and the third linear and nonlinear piezoelectric terms. The second equation describes the electrical (sensory) equilibrium of the piezoelectric laminate at a state (u, φ). In these equations, A_o is the midsurface and A_s is the shear stiffness matrix.

Equations (9) eventually provide a set of nonlinear equations, which, although might not be solved directly, they form the basis for the development of various iterative or searching solution techniques. The Newton–Raphson technique[21] is chosen because of its simplicity and also because it provides a linearized system of equations of motion. Equations (9) are further differentiated, and considering that δ expresses the variation of state variables u and φ they yield:

$$\begin{aligned}\{\delta u\}^T\{\mathrm{d}\Psi_u\} = -\int_{A_o} \Big(& \{\delta S^o\}^T[A]\{\mathrm{d}S^o\} + \{\delta S^o\}^T[B]\{\mathrm{d}k^o\} \\ & + \{\delta k^o\}^T[B]\{\mathrm{d}S^o\} + \{\delta k^o\}^T[D]\{\mathrm{d}k^o\} + \left\{\delta S_s^o\right\}^T[A_s]\left\{\mathrm{d}S_s^o\right\} \\ & + \{\delta S^L\}^T[A]\{\mathrm{d}S^o\} + \{\delta S^L\}^T[A]\{\mathrm{d}S^L\} + \{\delta S^L\}^T[B]\{\mathrm{d}k^o\} \\ & + \{\delta S^o\}^T[A]\{\mathrm{d}S^L\} + \{\delta k^o\}^T[B]\{\mathrm{d}S^L\} + \{\mathrm{d}\delta S^L\}^T[A]\{S^L\} \\ & + \{\mathrm{d}\delta S^L\}^T\Big([A]\{\mathrm{d}S^o\} + [B]\{\mathrm{d}k^o\} - \sum_m [\bar{E}^m]\{\mathrm{d}E^m\}\Big) \\ & + \sum_m \{\delta S^o\}^T[\bar{E}^m]\{\mathrm{d}E^m\} + \sum_m \{\delta k^o\}^T[\hat{E}^m]\{\mathrm{d}E^m\} \\ & + \sum_m \{\delta S^L\}^T[\bar{E}^m]\{\mathrm{d}E^m\} \Big) \,\mathrm{d}A\end{aligned}$$

$$\begin{aligned}\{\delta\varphi\}^T\{\mathrm{d}\Psi_e\} = -\int_{A_o} \Big(& \sum_m \{\delta E^m\}^T[\bar{E}^m]\{\mathrm{d}S^o\} \\ & + \sum_m \{\delta E^m\}^T[\hat{E}^m]\{\mathrm{d}k^o\} + \sum_m \{\delta E^m\}^T[\bar{E}^m]\{\mathrm{d}S^L\} \\ & + \sum_{mn} \{\delta E^m\}^T[G^{mn}]\{\mathrm{d}E^n\} \Big) \,\mathrm{d}A, \qquad m, n = 1, \ldots, L\end{aligned} \tag{10}$$

Finite Element Formulation

A finite element methodology for the analysis of composite piezoelectric plates is formulated, encompassing the precedings generalized nonlinear laminate mechanics. The state variables are approximated on the reference midplane A_o with local interpolation functions $N(x, y)$ of the following form:

$$u_j^o(x, y, t) = \sum_{i=1}^M u_j^{oi}(t) N^i(x, y), \qquad j = 1, \ldots, 3$$

$$\beta_j^o(x, y, t) = \sum_{i=1}^M \beta_j^i(t) N^i(x, y), \qquad j = 1, \ldots, 2$$

$$\varphi_j^m(x, y, t) = \sum_{i=1}^M \varphi^{mi}(t) N^i(x, y), \qquad m = 1, \ldots, L \tag{11}$$

where M is the number of element nodes indicated by superscript; L indicates the number of unknown electric potential values describing the layerwise representation through the laminate thickness. Thus a family of in-plane elements can be defined with five structural and L electric degrees of freedom per node, which include displacements $\boldsymbol{u}$, rotations $\boldsymbol{\beta}$, and electric potential $\boldsymbol{\varphi}^m$, respectively.

Combining Eqs. (4–7) with Eq. (11), substituting into Eq. (9), and collecting the common nodal displacement and electric potential terms, the following system of equations results:

$$\begin{aligned}\{\Psi_u(\boldsymbol{u}, \boldsymbol{\varphi})\} &= -[K_{\mathrm{uu}}(\boldsymbol{u}, \boldsymbol{\varphi})]\{u\} - [K_{\mathrm{ue}}(\boldsymbol{u}, \boldsymbol{\varphi})]\{\varphi\} + \{F\} \\ \{\Psi_e(\boldsymbol{u}, \boldsymbol{\varphi})\} &= -[K_{\mathrm{eu}}(\boldsymbol{u}, \boldsymbol{\varphi})]\{u\} - [K_{\mathrm{ee}}(\boldsymbol{u}, \boldsymbol{\varphi})]\{\varphi\} + \{Q\}\end{aligned} \tag{12}$$

At equilibrium $[\Psi_u(\boldsymbol{u}^*, \boldsymbol{\varphi}^*) = \Psi_e(\boldsymbol{u}^*, \boldsymbol{\varphi}^*) = 0]$ the preceding equations provide a discrete system of nonlinear equations, whereas away from equilibrium they yield the nodal imbalance force vector $\{\Psi_u\}$ between internal forces, actuator forces, and external loads, and the imbalance charge vector $\{\Psi_e\}$ between internal and external charges. The matrices $[K]$ with subscripts uu, ue, and ee indicate

the actual nonlinear stiffness, piezoelectric, and permittivity matrices of the plate. $\{F\}$ and $\{Q\}$ are the externally applied loads and charge vectors, respectively. The actual structural, piezoelectric, and permittivity matrices are expressed analytically by the following equations:

$$[K_{uu}(u,\varphi)] = \left[K^o_{uu}\right] + \left[K^L_{uu}\right] = \left[K^o_{uu}\right] + [P_1(\boldsymbol{u})]/2 + \left[P_2(\boldsymbol{u}^2)\right]/3$$
$$[K_{ue}(u,\varphi)] = \left[K^o_{ue}\right] + \left[K^L_{ue}\right] = \left[K^o_{ue}\right] + [P_3(\boldsymbol{u})]$$
$$[K_{eu}(u,\varphi)] = \left[K^o_{eu}\right] + \left[K^L_{eu}\right] = \left[K^o_{eu}\right] + [P_4(\boldsymbol{u})]/2$$
$$[K_{ee}(u,\varphi)] = \left[K^o_{ee}\right] \tag{13}$$

where superscripts o and L indicate linear and nonlinear components; $P_1(\boldsymbol{u})$ and $P_2(\boldsymbol{u}^2)$ indicate nonlinear stiffness terms, which depend linearly and quadratically on displacements, respectively; and $P_3(\boldsymbol{u})$ and $P_4(\boldsymbol{u})$ indicate the nonlinear piezoelectric matrices that depend linearly on displacements. The solution of the nonlinear system (12) is calculated iteratively using the Newton–Raphson method. Substituting Eqs. (4–7) together with Eq. (11) into Eq. (10) and after collecting the common terms, the linearized matrices for the nonlinear piezoelectric structure are obtained. These, in the context of a Newton–Raphson method, provide a coupled system of equations:

$$[\bar{K}_{uu}(u,\varphi)]\{\mathrm{d}u\} + [\bar{K}_{ue}(u,\varphi)]\{\mathrm{d}\varphi\} = \{\Psi_u(u,\varphi)\}$$
$$[\bar{K}_{eu}(u,\varphi)]\{\mathrm{d}u\} + [\bar{K}_{ee}]\{\mathrm{d}\varphi\} = \{\Psi_e(u,\varphi)\} \tag{14}$$

which yields a step $(\mathrm{d}\boldsymbol{u}, \mathrm{d}\boldsymbol{\varphi})$ toward the solution $(\boldsymbol{u}^*, \boldsymbol{\varphi}^*)$ of the nonlinear equations (12). The first equation describes the linearized structure behavior including actuator input, and the second equation describes the linearized sensory response about a point (u, φ).

The tangential structural, piezoelectric, and permittivity matrices contain the following terms:

$$[\bar{K}_{uu}(u,\varphi)] = \left[\bar{K}^o_{uu}\right] + \left[\bar{K}^\sigma_{uu}\right] + \left[\bar{K}^L_{uu}\right]$$
$$= \left[\bar{K}^\sigma_{uu}\right] + \left[\bar{K}^\sigma_{uu}\right] + [P_1(\boldsymbol{u})] + \left[P_2(\boldsymbol{u}^2)\right]$$
$$[\bar{k}_{ue}(u,\varphi)] = \left[\bar{K}^o_{ue}\right] + \left[\bar{K}^L_{ue}\right] = \left[\bar{K}^o_{ue}\right] + [P_3(\boldsymbol{u})]$$
$$[\bar{K}_{eu}(u,\varphi)] = \left[\bar{K}^o_{eu}\right] + \left[\bar{K}^L_{eu}\right] = \left[\bar{K}^o_{eu}\right] + [P_4(\boldsymbol{u})]$$
$$[\bar{K}_{ee}(u,\varphi)] = \left[\bar{K}^o_{ee}\right] \tag{15}$$

The tangential matrices have very similar structure and terms with the actual system matrices in Eq. (13). However, there is a new matrix appearing; this is the stress stiffness matrix K^σ_{uu}, which includes the effect of linear and nonlinear stress on the tangential stiffness matrix. More detailed definitions of the total and tangential matrices are provided in the Appendix.

An eight-node finite element was further developed, implementing quadratic Serendipity shape functions in the approximation of all nodal degrees of freedom shown in Eq. (11). The solution procedure just described and finite element matrices, specialized for the eight-node element, were encoded into prototype research software.

Numerical Results and Discussion

In this section, validations and evaluations of the developed models are presented for various active piezoelectric composite beams and plates. The materials considered were aluminum, graphite-epoxy composites, lead zirconate titanate (PZT5) piezoceramic, and polyvinylidene fluoride (PVDF) piezopolymer with properties shown in Table 1. The location of piezoelectric layers in the piezolaminate is indicated with letter p using standard laminate notation.

Validation Cases

Fully Clamped Plate

A square plate fully clamped at four edges ($E = 68.965$ Gpa and $v = 0.316$), with dimensions $L_x = L_y = 203$ mm and thickness $h = 2.032$ mm, subject to a uniform transverse pressure P was modeled, using a uniform 12×6 mesh of the present eight-node element. The predictions of the center deflection, normalized by the laminate thickness h, for various increments of the pressure, are shown in Fig. 2. In this and all subsequent figures, the line symbols indicate load increments. The present predictions are in excellent agreement with results reported by Palazotto and Dennis[22] using an eight-node higher-order shear element and with an analytical solution by Levy[23] based on a Fourier-series solution.

Table 1 Mechanical properties

Property	Gr/epoxy	Al	PZT-5	PVDF
Elastic properties				
E_{11}, GPa	132.4	66	62	4
E_{22}, GPa	10.8	66	62	4
G_{23}, GPa	3.6	27	18	1.54
G_{13}, GPa	5.6	27	23.6	1.54
G_{12}, GPa	5.5	27	23.6	1.54
ν_{12}	0.24	0.3	0.31	0.3
ν_{13}	0.24	0.3	0.31	0.3
ν_{23}	0.49	0.3	0.31	0.3
Piezoelectric coefficients (10^{-12} m/V)				
d_{31}	0	0	−220	−23
d_{32}	0	0	−220	−23
d_{24}	0	0	670	670
d_{15}	0	0	670	670
Electric permittivity				
$\varepsilon_{11}/\varepsilon_o$[a]	3.5	3.5	2598	12.43
$\varepsilon_{22}/\varepsilon_o$	3	3	2598	12.43
$\varepsilon_{33}/\varepsilon_o$	3	3	2598	12.43

[a] $\varepsilon_o = 8.85\ 10^{-12}$ farad/m, electric permittivity of air.

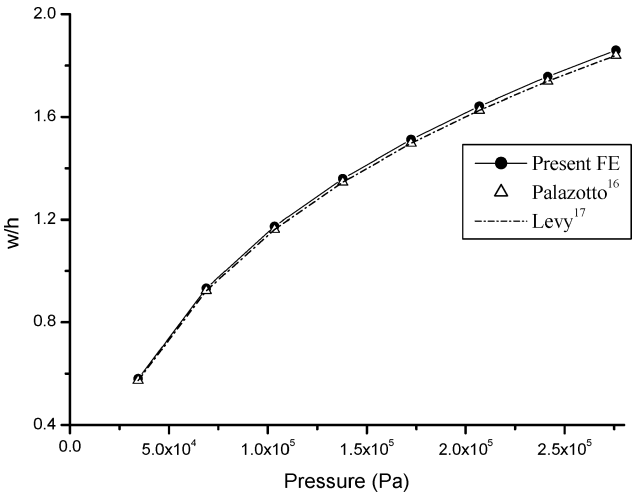

Fig. 2 Transverse deflection at center of an isotropic fully clamped plate loaded with transverse pressure.

Fully Hinged Plate

An orthotropic square composite plate, hinged in all four edges, with material properties $E_x = 20.68$ GPa, $E_y = 8.82$ GPa, $G_{12} = G_{13} = G_{23} = 2.5$ GPa, $v_{12} = v_{13} = v_{23} = 0.32$ and geometric dimensions $L_x = L_y = 304.8$ mm, $h = 3.5052$ mm was also analyzed using a uniform 8×8 mesh. Figure 3 shows the transverse deflection at the center of the plate for increasing values of applied uniform pressure. The deflections predicted by the present method are in excellent agreement with results reported by Reddy,[24] which lends further credence to the present finite element model.

Active Structures

Hinged Bilayer Piezoceramic Beam

The nonlinear quasi-static response of a [p/p] bimorph piezoceramic PZT-5 strip, hinged at both ends, which is subject to a combination of applied electric potential and uniform pressure, was examined. The length of the strip is $L_x = 200$ mm, the width $L_y = 20$ mm,

Table 2 Predicted center deflections for various uniform mesh densities in active beam cases

Finite element mesh	Center deflection w/h		
	[PZT5/PZT5] beam, $\varphi^A = 775$ V	[Al/PZT5] beam, $\varphi^A = 94.2$ V	
		with $P_3(u)$	w/o $P_3(u)$
4×1	0.888	0.519	0.265
10×1	0.901	0.519	0.265
20×1	0.902	0.519	0.265

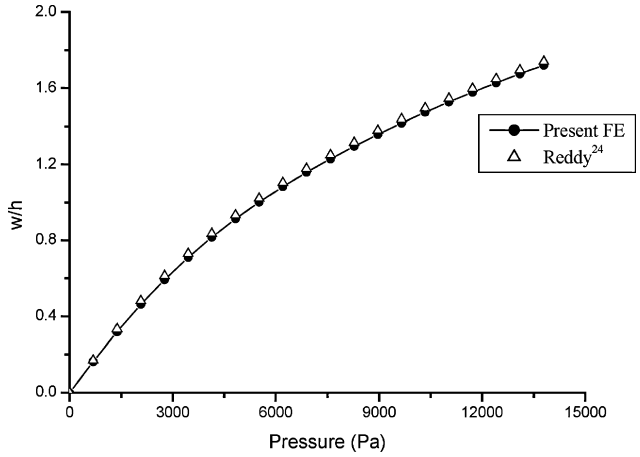

Fig. 3 Transverse deflection at center of an orthotropic fully hinged plate loaded with transverse pressure.

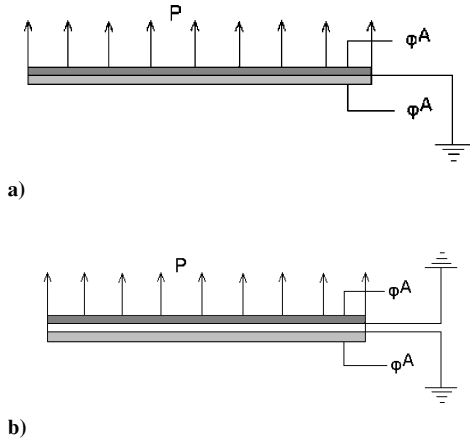

Fig. 4 Actuator and applied electric potential configurations: a) bimorph beam and b) composite beam or plate cross section with piezoelectric actuators attached on upper and lower surface.

and the thickness of each piezoelectric layer was $h_p = 0.5$ mm. The beam was modeled using a uniform mesh of 10×1 elements. Electric fields of opposite polarity were applied at each piezolayer, by applying electric potential φ^A-on the outer terminals of the piezoelectric layers, and 0 V at the inner terminal (Fig. 4a), such that a bending moment is effectively applied by the active layers. Figure 5 shows the deflection at the center of the beam for increasing values of applied electric potential, where the symbols indicate the applied electric potential increments used in the analysis. Table 2 shows the convergence of the predicted transverse deflection for various uniform mesh densities. The results indicate that the bimorph beam will exhibit a progressively increasing nonlinear behavior when high electric voltage is applied. The results show that the bending effectiveness of the actuators is progressively reduced at high deflection values, as if their active bending capability reaches a saturation plateau. For the case of symmetric actuator layup and pure active bending moment, as is the case of the present bimorph beam, this phenomenon is solely attributed to the membrane bending stiffening of the structure induced by the large rotation and represented in the nonlinear stiffness component K^L_{uu} [term P_2 in Eqs. (13) and (14)]. This saturation phenomenon in the active bending of the beam is more profound in the cases of preapplied mechanical pressure shown in Fig. 5; the latter increases the beam deflection and membrane bending stiffness, thus further reducing the bending deflection induced by the actuators. The results illustrate that active piezoelectric structures, even by assuming that their actuators behave withing their linear range as in the present model does, can actually exhibit very different active response when are forced to operate under large bending deflections.

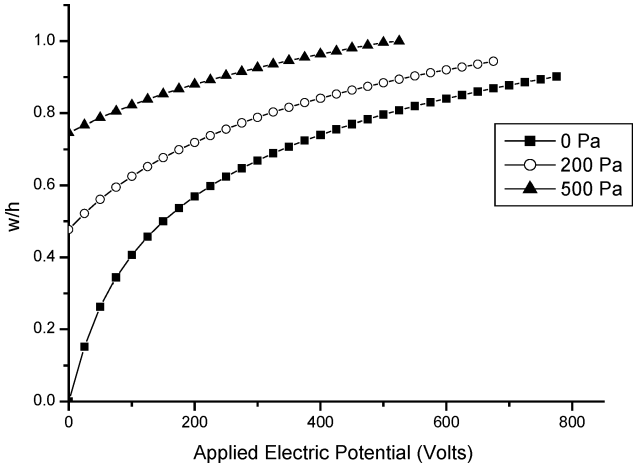

Fig. 5 Transverse center deflection of a hinged-hinged bimorph active strip.

Clamped-Free Bilayer Beam

A bimorph (PVDF/PVDF) cantilever beam, having the same dimensions as in the preceding case, was examined. The beam was modeled using a uniform mesh of 10×1 elements. Active bending is induced by applying opposite electric fields at each layer similarly to the preceding case (Fig. 4a). Figure 6a shows the predicted transverse tip displacement for various values of applied electric potential φ^A. The transverse deflection exhibits almost linear behavior because there are no in-plane stresses to stiffen the beam. Instead, the method predicts an in-plane deflection that varies nonlinearly with electric voltage, as seen in Fig. 6b. Linear theories do not predict an in-plane deflection, which again demonstrates one additional capability of the present nonlinear mechanics model.

Plates with Continuous Actuators

Four active square plates, simply supported on all sides with continuous PZT5 actuators attached on their free surfaces (Fig. 4b), were modeled having either an aluminum or Gr/epoxy laminated cross ply $[0_2/90_2]_s$, or quasi-isotropic $[0/90/45/-45]_s$ or unsymmetric $[45_2/-45_2]_2$ cores of equal thickness $h = 1$ mm. The dimensions of all plates were 203×203 mm, the ply thicknesses $h_l = 0.125$ mm, and the piezolayer thicknesses $h_p = 0.25$ mm. An 8×8 element uniform mesh model was used. A bending electric potential pattern of opposite polarity was applied on the actuators as shown in Fig. 4b, with φ^A V applied on the outer terminals of the actuators, and 0 V applied on the inner terminals. Figure 7 shows the displacement at the center of the various plates. The predicted behavior becomes highly nonlinear at intermediate and high values of applied potential. The nonlinearity is produced by the same mechanisms discussed in the beam cases, with the exception of the unsymmetric laminate were additional membrane bending coupling is introduced into $P_1(\boldsymbol{u})$ as a result of the nonzero coupling matrix $[B]$. The convergence rate of the finite element predictions for each case is shown in Table 3.

Plates with Actuator Patches

Similar active plate geometries and core laminations were considered, as in the preceding case, but the actuator layers have been

Table 3 Center deflections for various uniform mesh densities in active plate with continuous actuator layers ($\varphi^A = 2000$ V)

	Center deflection w/h			
Mesh	[PZT5/Al/PZT5]	$[PZT5/0_2/90_2]_s$	$[PZT5/0/90/45/-45]_s$	$[PZT5/(45_2/-45_2)_2/PZT5]$
4×4	1.900	2.293	2.015	1.838
8×8	1.976	2.420	2.133	1.942
12×12	1.991	2.437	2.154	1.959

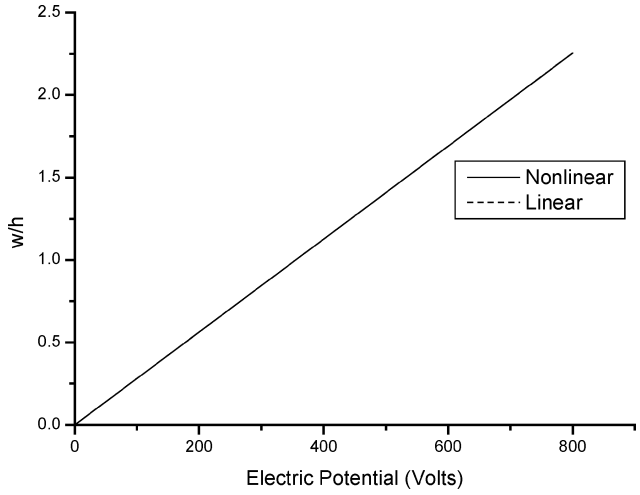

a)

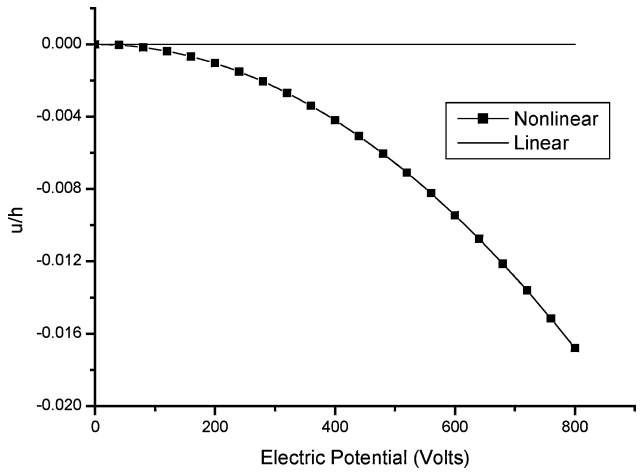

b)

Fig. 6 Predicted tip deflections of a cantilever bimorph (PVDF/PVDF) active beam: a) transverse deflection and b) axial deflection.

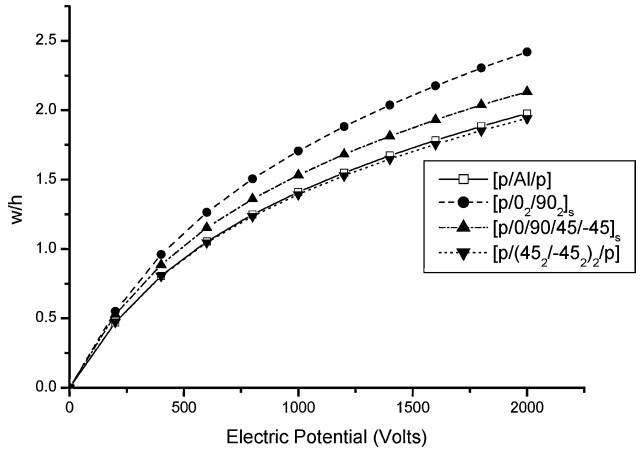

Fig. 7 Transverse center deflection of simply supported active plates with various laminate configurations and PZT5-actuators.

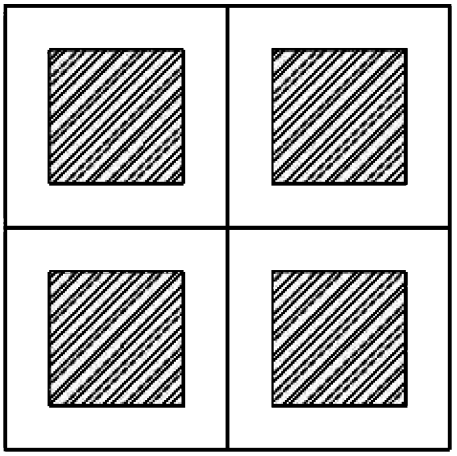

a)

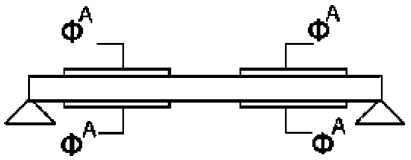

b)

Fig. 8 Schematic configuration of plate with piezoelectric patches attached on upper and lower surface: a) top and b) side view.

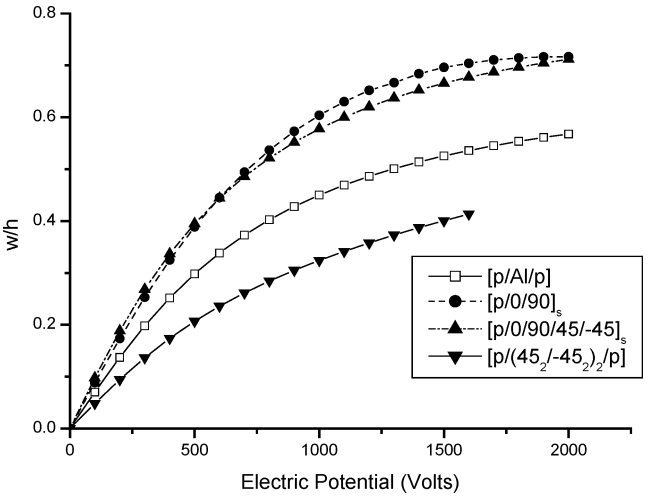

Fig. 9 Transverse center deflection of simply supported active plates with various laminate configurations and PZT5 patch actuators.

replaced with four piezoelectric patches covering 25% of the plate surface as shown in Fig. 8. All four patch pairs were identically loaded to induce bending moments. Finite element models with an 8×8 element mesh were used in all cases. Figure 9 shows the deflection (normalized by the total thickness of the laminate including the actuators) at the center of each plate, and as expected there is deviation from the results shown in Fig. 7. In this case, the actuator patches contribute less to the plate stiffness than the continuous actuator layers in the preceding cases, thus the actuator moment

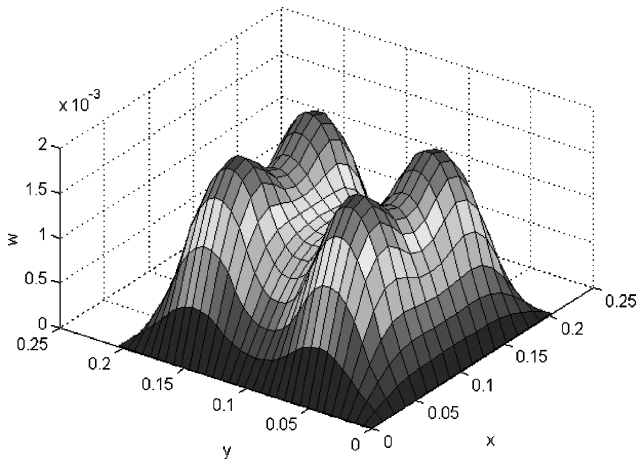

Fig. 10 Deformed shape of $[0_2/90_2]_s$ simply supported active plate with active piezoelectric patches at $\varphi^A = 2000$ V. All dimensions are in meters.

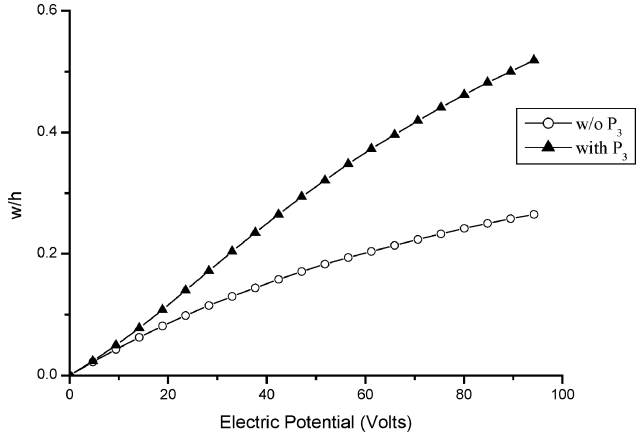

Fig. 11 Transverse center deflection of a hinged-hinged active asymmetric [Al/p] strip with a single continuous actuator attached on the upper surface.

is received mainly by the composite core stiffness, resulting in a more flexible configuration that seemingly behaves nonlinearly at lower deflection values. Figure 10 shows the deformed shape of the $[0_2/90_2]$ plate at the end of the load path ($\varphi^A = 2000$ V). The deformation appears highly nonuniform and changes slowly in shape with further increasing applied electric potential values.

Beam with Asymmetric Actuator

The active response of a hinged-hinged asymmetric [Al/p] composite beam $L_x = 200$ mm, $L_y = 20$ mm, with a PZT-5 layer attached on the upper surface is predicted, using a uniform 10×1 mesh. The thickness of the aluminum was 0.75 mm and of the piezolayer 0.25 mm. An electric voltage φ^A is imposed on the upper terminal while the inner terminal remained grounded; thus, both in-plane and bending loads were induced by the actuator. In the case of actuators placed through the thickness or loaded such that an average in-plane force is applied, as in the present case of the single actuator, the nonlinear piezoelectric component $[K^L_{ue}] = [P_3(\boldsymbol{u})]$ becomes nonzero at high rotation angles $w_{,x}$, $w_{,y}$, and physically corresponds to an active nonlinear force component acting along the thickness direction z. Figure 11 shows the center deflection of the active beam vs the applied electric potential for cases where the piezoelectric matrix includes 1) only the linear terms K^o_{ue} and 2) both K^o_{ue} and $P_3(\boldsymbol{u})$ matrices. In both cases, the induced stress by the piezoactuator applies a bending moment and an in-plane force, causing the transverse deflection seen in Fig. 11 for $P_3(\boldsymbol{u}) = 0$. The difference predicted with the inclusion of $P_3(\boldsymbol{u})$, however, represents the effect of a third nonlinear active force, acting transversely to the beam at high rotations. Thus, the results in Fig. 11 illustrate that in addition to the nonlinear

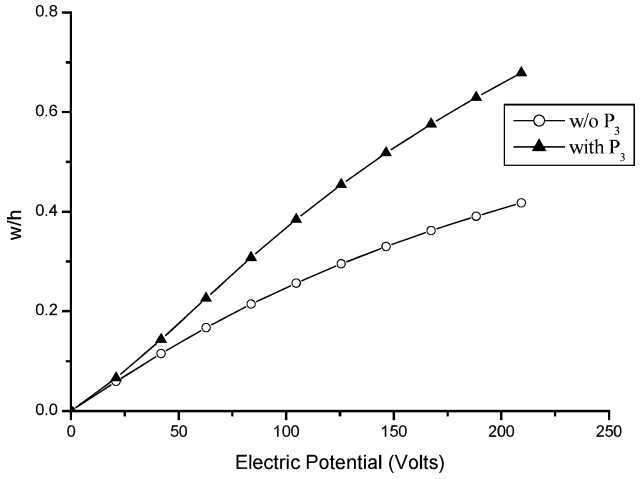

Fig. 12 Transverse center deflection of a fully hinged [0/90/45/−45/p] active asymmetric plate with a continuous actuator attached on the upper surface.

membrane-bending stiffening effects (term K^L_{uu}), investigated in the preceding cases of pure bending actuation, the nonlinear piezoelectric component K^L_{ue} can also significantly affect the active structural response. A third type of nonlinear effect is also depicted in Fig. 11; this is a nonlinear loss in flexural stiffness induced by the active in-plane force and expressed by the tangential stress stiffness matrix K^σ_{uu} in Eq. (15) resulting in the onset of buckling, but this issue will be investigated in future work. Table 2 illustrates the very good convergence rate of the present finite element method in predicting this type of nonlinear response.

Hinged Plate with Asymmetric Actuators

The case of a fully hinged asymmetric [0/90/45/−45/p] active plate with a continuous piezoelectric active layer attached on the upper surface is examined. The dimensions of the plate are identical to those in the preceding cases. The thickness of each composite ply is 0.25 mm and of the piezoelectric layer 0.25 mm. An 8×8 element uniform mesh model was used. This is seemingly the most complex case considered thus far, involving all of the nonlinear stiffness and piezoelectric terms of the formulation, shown in Eqs. (13) and (15), as a result of the asymmetry in laminate and actuator configuration. Most comments in the preceding case regarding the multiple sources of nonlinearity, also apply here. Figure 12 shows the center deflection of the plate as function of the applied actuator voltage with and without consideration of the nonlinear piezoelectric matrix $P_3(\boldsymbol{u})$. Similarly to the preceding case, the absence of the nonlinear piezoelectric matrix component $P_3(\boldsymbol{u})$ can result in significant underestimation of the active structure response.

In closing, all preceding numerical examples have demonstrated the new capabilities introduced by the present nonlinear mechanics framework and finite element methodology into the analysis of active piezoelectric plate structures. They have also illustrated the strong nonlinear effects exerted on such structures when the latter are subject to large rotation deformations. These effects should not be confused with effects induced by the nonlinear behavior of the piezoelectric elements, which are not included herein and can be addressed in the future.

Summary

A theoretical framework was presented for the coupled nonlinear response of laminated plate structures with nonlinear geometric effects caused by large rotations, entailing laminate mechanics and a finite element solution. Emphasis was placed on active nonlinear plate structures. Based on this framework, an eight-node nonlinear plate element was developed and encoded into a research code, enabling realistic predictions of the quasi-static nonlinear response of composite beams and plates with piezoelectric actuators. Evaluation results were presented for various active beams and plate

configurations. The results have demonstrated the progressively increasing strong nonlinear behavior of active structures at large bending deflections, driving the active bending response in a saturation region. The dependence of linear active response on the piezolaminate configuration was also demonstrated. Finally, the onset of a new active force/pressure component at large bending rotations acting transversely to the plate was predicted for the case of non-purely bending actuation, and its contribution on the transverse deflection was quantified.

Overall, the results illustrate the significance of the nonlinear active behavior in piezoelectric adaptive structures caused by large displacements and highlight the value and quality of the present theory and finite element method. Future work can focus on experimental demonstrations, on the extension of the present work on nonlinear sensory structures, and on the buckling and postbuckling behavior of adaptive structures.

Appendix: Linear and Nonlinear Finite Element Matrices

Tangential terms [Eq. (15)]:

$$\delta \boldsymbol{u}^T \left[\bar{K}^o_{\mathrm{uu}}\right] \mathrm{d}\boldsymbol{u} = \int_{A_o} \Big(\{\delta S^o\}^T [A] \{\mathrm{d}S^o\} + \{\delta S^o\}^T [B] \{\mathrm{d}k^o\} + \{\delta k^o\}^T [B] \{\mathrm{d}S^o\} + \{\delta k^o\}^T [D] \{\mathrm{d}k^o\} + \{\delta S^o\}^T [A_s] \{\mathrm{d}S^o\} \Big) \, \mathrm{d}A$$

$$\delta \boldsymbol{u}^T \left[\bar{K}^\sigma_{\mathrm{uu}}\right] \mathrm{d}\boldsymbol{u} = \int_{A_o} \{\mathrm{d}\delta S^L\}^T \left([A] \{\mathrm{d}S^o\} + [B] \{\mathrm{d}k^o\} - \sum_m [\bar{E}^m] \{\mathrm{d}E^m\} \right) \mathrm{d}A$$

$$\delta \boldsymbol{u}^T \left[\bar{K}^L_{\mathrm{uu}}\right] \mathrm{d}\boldsymbol{u} = \int_{A_o} (\{\delta S^L\}^T [A] \{\mathrm{d}S^o\} + \{\delta S^L\}^T [B] \{\mathrm{d}k^o\} + \{\delta S^o\}^T [A] \{\mathrm{d}S^L\} + \{\delta k^o\}^T [B] \{\mathrm{d}S^L\}) \, \mathrm{d}A$$

$$\delta \boldsymbol{u}^T \left[\bar{K}^L_{\mathrm{uu}}\right] \mathrm{d}\boldsymbol{u} = \int_{A_o} (\{\delta S^L\}^T [A] \{\mathrm{d}S^L\} + \{\mathrm{d}\delta S^L\}^T [A] \{S^L\}) \, \mathrm{d}A$$

$$\delta \boldsymbol{u}^T \left[\bar{K}^o_{\mathrm{ue}}\right] \mathrm{d}\boldsymbol{\varphi} = \int_{A_o} (\{\delta S^o\}^T [\bar{E}^m] \{\mathrm{d}E^m\} + \{\delta k^o\}^T [\hat{E}^m] \{\mathrm{d}E^m\}) \, \mathrm{d}A$$

$$\delta \boldsymbol{u}^T \left[\bar{K}^L_{\mathrm{ue}}\right] \mathrm{d}\boldsymbol{\varphi} = \int_{A_o} (\{\delta S^L\}^T [\bar{E}^m] \{\mathrm{d}E^m\}) \, \mathrm{d}A$$

$$\delta \boldsymbol{\varphi}^T \left[\bar{K}^o_{\mathrm{eu}}\right] \mathrm{d}\boldsymbol{u} = \int_{A_o} (\{\delta E^m\}^T [\bar{E}^m] \{\mathrm{d}S^o\} + \{\delta E^m\}^T [\hat{E}^m] \{\mathrm{d}k^o\}) \, \mathrm{d}A$$

$$\delta \boldsymbol{\varphi}^T \left[\bar{K}^L_{\mathrm{eu}}\right] \mathrm{d}\boldsymbol{u} = \int_{A_o} (\{\delta E^m\}^T [\bar{E}^m] \{\mathrm{d}S^L\}) \, \mathrm{d}A$$

$$\delta \boldsymbol{\varphi}^T \left[\bar{K}^o_{\mathrm{ee}}\right] \mathrm{d}\boldsymbol{\varphi} = \int_{A_o} (\{\delta E^m\}^T [G^{mn}] \{\mathrm{d}E^n\}) \, \mathrm{d}A$$

Actual matrix terms [Eq. (13)]:

$$\delta \boldsymbol{u}^T \left[\bar{K}^o_{\mathrm{uu}}\right] \boldsymbol{u} = \int_{A_o} \Big(\{\delta S^o\}^T [A] \{S^o\} + \{\delta S^o\}^T [B] \{k^o\} + \{\delta k^o\}^T [B] \{S^o\} + \{\delta k^o\}^T [D] \{k^o\} + \{\delta S^o\}^T [A_s] \{S^o\} \Big) \, \mathrm{d}A$$

$$\delta \boldsymbol{u}^T \left[\bar{K}^L_{\mathrm{uu}}\right] \boldsymbol{u} = \int_{A_o} (\{\delta S^L\}^T [A] \{S^o\} + \{\delta S^L\}^T [B] \{k^o\} + \{\delta S^o\}^T [A] \{S^L\} + \{\delta k^o\}^T [B] \{S^L\}) \, \mathrm{d}A$$

$$\delta \boldsymbol{u}^T \left[\bar{K}^L_{\mathrm{uu}}\right] \boldsymbol{u} = \int_{A_o} (\{\delta S^L\}^T [A] \{S^L\}) \, \mathrm{d}A$$

$$\delta \boldsymbol{u}^T \left[\bar{K}^o_{\mathrm{ue}}\right] \boldsymbol{\varphi} = \int_{A_o} (\{\delta S^o\}^T [\bar{E}^m] \{E^m\} + \{\delta k^o\}^T [\hat{E}^m] \{E^m\}) \, \mathrm{d}A$$

$$\delta \boldsymbol{u}^T \left[\bar{K}^L_{\mathrm{ue}}\right] \boldsymbol{\varphi} = \int_{A_o} (\{\delta S^L\}^T [\bar{E}^m] \{E^m\}) \, \mathrm{d}A$$

$$\delta \boldsymbol{\varphi}^T \left[\bar{K}^o_{\mathrm{eu}}\right] \boldsymbol{u} = \int_{A_o} (\{\delta E^m\}^T [\bar{E}^m] \{S^o\} + \{\delta E^m\}^T [\hat{E}^m] \{k^o\}) \, \mathrm{d}A$$

$$\delta \boldsymbol{\varphi}^T \left[\bar{K}^L_{\mathrm{eu}}\right] \boldsymbol{u} = \int_{A_o} (\{\delta E^m\}^T [\bar{E}^m] \{S^L\}) \, \mathrm{d}A$$

$$\delta \boldsymbol{\varphi}^T \left[\bar{K}^o_{\mathrm{ee}}\right] \boldsymbol{\varphi} = \int_{A_o} (\{\delta E^m\}^T [G^{mn}] \{E^n\}) \, \mathrm{d}A$$

Acknowledgment

This work was partially funded through the Karatheodoris Program of the Research Office of the University of Patras. This support is gratefully acknowledged.

References

[1]Saravanos, D. A., and Heyliger, P. R., "Mechanics and Computational Models for Laminated Piezoelectric Beams, Plates and Shells," *Applied Mechanics Reviews*, Vol. 52, 1999, pp. 305–320.

[2]Crawley, E. F., and Lazarus, K. B., "Induced Strain Actuation of Isotropic and Anisotropic Plates," *AIAA Journal*, Vol. 29, 1991, pp. 944–951.

[3]Lee, C. K., and Moon, F. C., "Laminated Piezopolymer Plates for Torsion and Bending Sensors and Actuators," *Journal of the Acoustical Society of America*, Vol. 85, 1989, pp. 2432–2439.

[4]Tzou, H. S., and Zhong, J. P., "Electromechanics and Vibrations of Piezoelectric Shell Distributed Systems," *Journal of Dynamic Systems, Measurement, and Control*, Vol. 115, 1993, pp. 506–517.

[5]Robins, D., and Reddy, J., "Analysis of Piezoelectrically Actuated Beams Using a Layerwise Displacement Theory," *Computers and Structures*, Vol. 41, 1991, pp. 265–279.

[6]Chattopadhyay, A., Gu, H., and Daescu, D. D., "Dynamics of Delaminated Composite Plates with Piezoelectric Actuators," *AIAA Journal*, Vol. 37, 1999, pp. 248–254.

[7]Saravanos, D. A., and Heyliger, P. R., "Coupled Layerwise Analysis of Composite Beams with Embedded Piezoelectric Sensors and Actuators," *Journal of Intelligent Material Systems and Structures*, Vol. 6, 1995, pp. 350–363.

[8]Saravanos, D. A., "Coupled Mixed-Field Laminate Theory and Finite Element for Smart Piezoelectric Composite Shell Structures," *AIAA Journal*, Vol. 35, 1997, pp. 1327–1333.

[9]Mitchell, J. A., and Reddy, J. N., "A Refined Hybrid Plate Theory for Composite Laminates with Piezoelectric Laminae," *International Journal of Solids and Structures*, Vol. 32, 1995, pp. 2345–2367.

[10]Heyliger, P., "Static Behavior of Laminated Elastic Piezoelectric Plates," *AIAA Journal*, Vol. 32, 1994, pp. 2481–2484.

[11]Heyliger, P. R., "Exact Solutions for Simply-Supported Laminated Piezoelectric Plates," *Journal of Applied Mechanics*, Vol. 64, 1997b, pp. 299–306.

[12]Fripp, L. R., and Hagood, N. W., "Distributed Structural Actuation with Electrostrictors,"*Journal of Sound and Vibration*, Vol. 203, 1996, pp. 11–40.

[13]Debus, J. C., Dubus, B., and Coutte, J., "Finite Element Modelling of Lead Magnesium Niobate Electrostrictive Materials-Static Analysis," *Journal of the Acoustical Society of America*, Vol. 103, 1998, pp. 3336–3343.

[14]Lee, H. J., and Saravanos, D. A., "The Effect of Temperature Dependent Material Properties on the Responnse of Piezoelectric Composite Materials," *Journal of Intelligent Material Systems and Structures*, Vol. 9, 1998, pp. 503–508.

[15]Thornburgh, R. P., and Chattopadhyay, A., "Nonlinear Actuation of Smart Composites Using a Coupled Piezoelectric-Mechanical Model," *Smart Materials and Structures*, Vol. 10, 2001, pp. 743–749.

[16]Pai, P. F., Nayfeh, A. H., Oh, K., and Mook, D. T., "A Refined Nonlinear Model of Composite Plates with Integrated Piezoelectric Actuators and Sensors," *International Journal of Solids and Structures*, Vol. 30, 1993, pp. 1603–1630.

[17]Tzou, H. S., and Bao, Y., "Nonlinear Piezothermoelasticity and Multi-Field Actuations, Part1: Nonlinear Anisotropic Piezothermoelastic Shell Laminates," *Journal of Vibration and Acoustics*, Vol. 119, 1997, pp. 374–381.

[18]Tzou, H. S., and Zhou, Y. H., "Nonlinear Piezothermoelasticity and Multi-Field Actuations, Part 2: Control of Nonlinear Deflection, Buckling and Dynamics," *Journal of Vibration and Acoustics*, Vol. 119, 1997, pp. 382–389.

[19]Oh, I. K., Han, J. H., and Lee, I., "Thermopiezoelastic Snapping of Piezolaminated Plates Using Nonlinear Finite Elements," *AIAA Journal*, Vol. 39, 2001, pp. 1188–1198.

[20]Mukherjee, A., and Chaudhouri, A. S., "Piezolaminated Beams with Large Deformations," *International Journal of Solids and Structures*, Vol. 39, 2002, pp. 4567–4582.

[21]Zienkiewicz, O. C., "Non-Linear Material Problems. Plasticity, Creep (Visco-plasticity), Non-Linear Field Problems," *The Finite Element Method*, McGraw–Hill, Berkshire, England, U.K., 1977, pp. 452–454.

[22]Palazotto, A. N., and Dennis, S. T., "Geometrically Nonlinear Plate Solutions," *Nonlinear Analysis of Shell Structures*, AIAA, Washington, DC, 1992, pp. 139, 140.

[23]Levy, S., "Square Plate with Clamped Edges Under Normal Pressure Producing Large Deflections," NACA TN-847, July 1942.

[24]Reddy, J. N., "Nonlinear Analysis of Composite Laminates," *Mechanics of Laminated Composite Plates*, CRC Press, Boca Raton, FL, 1997, pp. 736, 737.

A. Chattopadhyay
Associate Editor